International Journal of Nanomedicine

Dovepress
open access to scientific and medical research

Open Access Full Text Article

ORIGINAL RESEARCH

Long-lasting bactericidal activity through selective physical puncture and controlled ions release of polydopamine and silver nanoparticles–loaded TiO_2 nanorods in vitro and in vivo

Ming Guan[1,2,*]
Yangmengfan Chen[1,*]
Yong Wei[3]
Hao Song[3]
Chenghao Gao[1]
Hao Cheng[4]
Yong Li[1]
Kaifu Huo[5]
Jijiang Fu[3]
Wei Xiong[1]

[1]Department of Orthopedics, Tongji Hospital, Tongji Medical College, Huazhong University of Science and Technology, Wuhan 430030, People's Republic of China; [2]Department of Biologic and Materials Sciences, University of Michigan, Ann Arbor, MI 48109-1078, USA; [3]The State Key Laboratory of Refractories and Metallurgy, Wuhan University of Science and Technology, Wuhan 430081, People's Republic of China; [4]Department of Orthopedic Surgery, Nanfang Hospital, Southern Medical University, Guangzhou 510515, People's Republic of China; [5]Wuhan National Lab for Optoelectronics, Huazhong University of Science and Techonology, Wuhan 430074, People's Republic of China

*These authors contributed equally to this work

Correspondence: Jijiang Fu
The State Key Laboratory of Refractories and Metallurgy, Wuhan University of Science and Technology, Wuhan 430081, People's Republic of China
Tel +860 276 886 2529
Email fujijiang@wust.edu.cn

Wei Xiong
Department of Orthopedics, Tongji Hospital, Tongji Medical College, Huazhong University of Science and Technology, 1095 Jiefang Avenue, Wuhan 430030, People's Republic of China
Tel +860 278 366 5219
Email xcxgreatwellus@hotmail.com

This article was published in the following Dove Press journal:
International Journal of Nanomedicine

Background: Titanium (Ti) implant-associated infection, which is mostly caused by bacterial adhesion and biofilm formation, may result in implant failure and secondary surgery. Thus it is an urgent issue to prevent bacterial infections at the earliest step.

Purpose: To develop a novel surface strategy of polydopamine (PDA) and silver (Ag) nanoparticle-loaded TiO_2 nanorods (NRDs) coatings on Ti alloy.

Materials and methods: Ag-TiO_2@PDA NRDs was fabricated on Ti alloy by hydrothermal synthesis. The antibacterial activity of Ag-TiO_2@PDA NRDs against *Escherichia coli* and methicillin-resistant *Staphylococcus aureus* were tested by FE-SEM, Live/Dead staining, zone of inhibition, bacteria counting method and protein leakage analysis *in vitro*. In addition, an implant infection model was conducted and the samples were tested by X-ray, Micro-CT and histological analysis *in vivo*. Besides, cell morphology and cytotoxicity of Mouse calvarial cells (MC3T3-E1) were characterized by FE-SEM, immunofluorescence and CCK-8 test *in vitro*.

Results: Our study successfully developed a new surface coating of Ag-TiO_2@PDA NRDs. The selective physical puncture of bacteria and controlled release of Ag+ ions of Ag-TiO_2@PDA NRDs achieved a long-lasting bactericidal ability and anti-biofilm activity with satisfied biocompatibility.

Conclusion: This strategy may be promising for clinical applications to reduce the occurrence of infection in the implant surgeries

Keywords: bacterial infection, polydopamine, silver nanoparticles, physical puncture, TiO_2 nanorods, bactericidal activity

Introduction

With the development of modern medical implants, titanium (Ti) alloy has been commonly applied in the field of orthopedics and dentistry, because of their excellent mechanical properties, biocompatibility, and chemical stability.[1] However, two major concerns of bacterial infections and poor osseointegration have been remained to be effectively resolved.[2,3] Implant infection, which is mostly caused by the bacterial adhesion and biofilm formation, may result in implant failure and secondary surgery.[4] Since the biofilms are the physical barriers, which is composed by a three-dimension extracellular polymeric matrix, to protect the inside bacteria from attack by host defense and antibiotics.[5] As a result, 1,000-fold higher antibiotic dosage and

submit your manuscript | www.dovepress.com
DovePress
http://doi.org/10.2147/IJN.S202625

extended antibiotic therapy may be required to kill the bacteria in biofilm than the common planktonic bacteria, especially for the antibiotics-resistant bacteria strain like methicillin-resistant *Staphylococcus aureus* (MRSA), etc.[6,7] Therefore, it is an urgent issue to inhibit the formation of biofilm at the earliest step by using physical and/or chemical methods.[8] By far, there are three main categories of antimicrobial surfaces: (a) bactericidal element content releasing from coatings, such as the bactericide ion release; (b) contact-killing coatings, such as the surface nanostructure of the cicada wing; and (c) anti-adhesion coatings, such as PEG, zwitterion and physical surface modifications.[9] While inhibiting bacterial adhesion, Ti implants may not promote the spreading and attachment of osteoblasts, resulting in poor osseointegration and implant loosening.[10]

Silver (Ag) with the properties of vast spectrum bactericidal activity and anti-biofilm effect has been widely applied from ancient times.[6] However, the occurrence of burst release remains one of the biggest concerns of the biomaterial, which invokes a considerable level of cytotoxicity.[11] Besides, in order not to compromise the material biocompatibility, the appropriate concentration range for Ag^+ ions was reported between 100 ppb and 10 ppm in a biological solution, which was tough for the control of ion releasing.[12] These challenges have prompted researchers to develop new strategies for the adequate antibacterial ability and proper biocompatibility in implant applications.

Polydopamine (PDA) has been commonly used to modify the surface characteristics of biomaterial scaffolds as an important platform and stabilization agent, with excellent biocompatibility, biodegradability, and hydrophilicity.[13,14] Meanwhile, as the desirable adhesion agent for biological reagents,[15] the o-diphenol and amine groups of PDA may modify the Ag^+ ions burst release pattern to long-lasting release pattern by the chelation bonding of Ag nanoparticles.[16,17] Moreover, PDA has been reported to promote the spreading and attachment of pre-osteoblast by engaging and activating cell membrane receptors.[18,19]

It has been reported that the specific surface topographies with patterns smaller than bacterial cells possessed a broad-spectrum bactericidal ability.[20] For example, the particular surface nanostructure of cicada wings was reported to have the outstanding bactericidal effect by mechanically rupturing of attached cells within 3 mins.[21,22] Therefore, based on hydrothermal synthesis, TiO_2 nanorods (NRDs) coatings fabricated on Ti implants may provide a new strategy to combat implant infection.

Our current research aims to produce a new surface strategy, namely the Ag-TiO_2@PDA NRDs, with the properties of selective physical puncture of bacteria and long-lasting Ag^+ ions release for the balance of the bactericidal activity and cytotoxicity. Through a series of in vitro and in vivo tests, it resulted that the Ag-TiO_2@PDA NRDs coatings possessed the long-term anti-bacterial and anti-biofilm capacities.

Materials and methods

Specimen preparation

As illustrated in Figure 1, Ti foils (10 mm×10 mm×1 mm) and Ti rods (diameter: 1 mm; length: 10 mm) were purchased and polished by SiC sandpapers, followed by degreasing sequentially with acetone, ethanol, and distilled water, and then dried by nitrogen gas. Later, the samples were loaded in a Teflon-lined autoclave with adequate 1 M NaOH and heated for 10 h in a sealed autoclave (200°C) to fabricate sodium titanate NRDs on the Ti foil, followed by ultrasonic washing. Then, the sodium titanate NRDs were subjected to a hydrogen ion exchange process

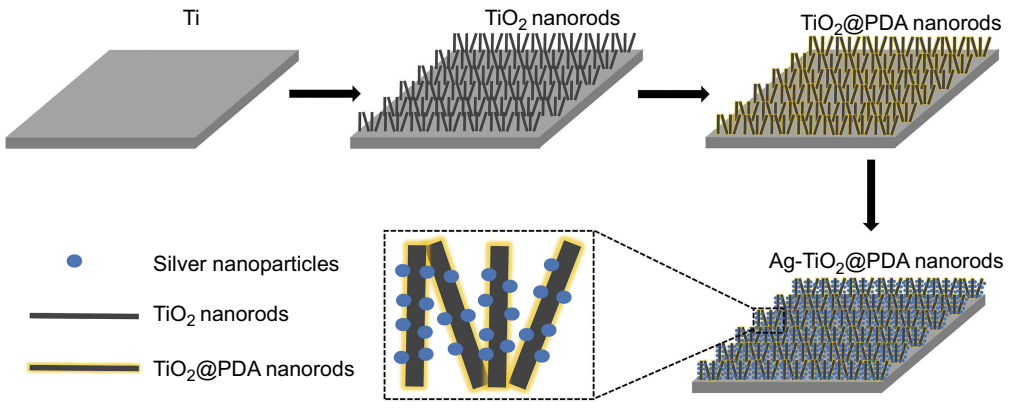

Figure 1 Schematic diagram of fabrication process of Ag-TiO_2@PDA nanorods coatings.

in diluted hydrochloric acid (HCl) for 1 hr to obtain the titanic acid NRDs. After washed by deionized water and dried at 60°C, the products were annealed at 400°C for 2 hrs in the air to fabricate TiO_2 NRDs specimens.

To prepare the PDA-coated TiO_2 NRDs (denoted as TiO_2@PDA NRDs), the as-prepared TiO_2- NRDs specimens were immersed into a Tris-buffer solution (10 mM, 100 mL), and then 100 mg of dopamine hydrochloride was dispersed into the solution with magnetic stirring for 6 hrs. After washed with deionized water three times, the resultant TiO_2@PDA NRDs were dried at 60°C. Then, the TiO_2 @PDA NRDs specimens were soaked in the $AgNO_3$ solution (100 mM) for 15 mins and irradiated with ultraviolet light by a high-pressure Hg lamp for 30 mins to obtain Ag nanoparticles–loaded TiO_2@PDA NRDs (denoted as Ag-TiO_2@PDA NRDs). For comparison, the Ag nanoparticles–loaded TiO_2 NRDs (denoted as Ag-TiO_2 NRDs) were prepared in the same procedure except for PDA coatings.

All the samples were cleaned by sequential ultrasonic, dried by air, and sterilized by ultraviolet light in sequence before antibacterial tests.

Sample surface characterization

The surface morphology of samples was measured by a field emission scanning electron microscopy (FE-SEM; FEI Nova 400 Nano, USA) and the microstructure of Ag-TiO_2@PDA NRDs was measured by a transmission electron microscopy (TEM; Tecnai G20, FEI, USA). The surface chemical composition and elemental analysis were evaluated by energy dispersive X-ray (EDX) spectrum and X-ray photoelectron spectroscopy (XPS; ESCALAB MK-II, VG, USA). The hydrophilicity of the samples was measured by the water contact angle (DSA1 System, Kruss, Germany).

Ag^+ ions release into PBS

The Ag-TiO_2 NRDs and Ag-TiO_2@PDA NRDs samples were immersed in 6 mL of PBS for 1, 3, 6, 10, and 14 days, and PBS was refreshed every 24 hrs. Then, the liquid was collected and evaluated by inductively coupled plasma atomic emission spectrometry (ICP-AES; IRIS Advantage ER/S) with a specific emission line at 328.1 nm for Ag.[6]

Antibacterial activity in vitro

The antibacterial activities against gram-positive MRSA and gram-negative *Escherichia coli* (*E. coli*) were measured by FE-SEM, Live/Dead staining, zone of inhibition (ZOI), bacteria counting method, and protein leakage analysis in vitro.

Firstly, the bactericidal and antibiofilm formation ability was tested by FE-SEM and fluorescence observation. We placed the samples on a 24-well plate and immersed them in 1 mL bacteria suspension (1.5×10^4 colony-forming units [CFU_S]/mL) in the standard Luria-Bertani culture medium each well for 24 hrs culturing at 37°C. Then, the samples were washed by PBS three times to remove non-adhesion bacteria, fixed with 2.5% glutaraldehyde solution at 4°C for 4 hrs, and dehydrated in ethanol series (30%, 45%, 75%, 95%, and 100%) for 15 mins sequentially. After coated with Au in a sputter coater, the dried samples were captured by FE-SEM eventually. Similarly, the specimens were stained with the Live/Dead *BacLight* Bacterial Viability Kit (cat# L7007; Invitrogen) for 15 mins after co-cultured with MRSA for 24 and 48 hrs and then imaged by the fluorescence microscope. Thus, intact cell membranes would be stained fluorescent green by SYTO 9 and damaged cell membranes would be stained fluorescent red by propidium iodide.

Secondly, the ZOI was conducted to test the antiplanktonic bacteria ability. We placed respective samples onto M-H plates, which was inoculated by 20 μL bacterial suspension (1.5×10^8 CFU_S/mL) at 37°C for 24 hrs of incubation to observe zone inhibition diameter.

Thirdly, the bacteria counting method was conducted to evaluate the anti-adhesion bacterial rate. After co-cultured with 1 mL bacterial suspension (1.5×10^4 CFU_S/mL^{-1}) at 37°C for 24 hrs, the samples were collected in 1 mL of sterile PBS. The samples were dislodged by sonication at 50 Hz for 2 mins to remove the adhered bacteria. Then, the dissociated bacterial suspension was gradient diluted with sterile PBS and plated on M-H agar at 37°C. After 24 hrs of incubation, the active bacteria were counted carefully and the anti-adherent bacteria effect was represented by the antibacterial ratio based on the following formulas: antibacterial ratio (%)=(B–A)/B×100%, where A is the mean number of active bacteria inoculated with the experimental groups (CFU/sample), and B is the mean number of active bacteria inoculated with the pure Ti group (CFU/sample). The bacterial counting method was conducted among Ti, TiO_2 NRDs and TiO_2@PDA NRDs groups for 1 day and Ti, Ag-TiO_2 NRDs and Ag-TiO_2@PDA NRDs groups for 1, 7 and 14 days to analyze the long-term anti-adherent bacterial ability.

Lastly, the protein concentration of bacterial suspension was measured by an Enhanced BCA Protein Assay Kit to test the potential protein leakage of bacterial cytoplasm.

Cell morphology and cytotoxicity evaluation in vitro

An mouse calvarial cells line (MC3T3-E1) was obtained from the Chinese Academy of Sciences Shanghai cell bank. MC3T3-E1 cells (5×10^4 cells/cm^2) were cultured in a 24-well plate each well. The cell morphology was imaged by the fluorescence microscopy and FE-SEM. After incubation for 1 day, the samples were washed with sterile PBS three times and fixed in 2.5% glutaraldehyde solution at 4°C for 4 hrs. Then, the samples were stained by phalloidin (Sigma, USA) for 50 mins in the dark environment and DAPI for 10 mins and then imaged by the fluorescence microscope. The same FE-SEM procedures described above were adopted to observe the morphology of bacteria.

A CCK-8 kit (Boster Biological Technology Co., CA, USA) was used to test the cytotoxicity level for cell cultures on various samples. MC3T3-E1 cells (3×10^4 cells/cm^2) were seeded on the samples and cultured for 24 hrs in a 24-well plate each well at 5% CO_2 and 37°C. Then, the CCK-8 solution was added to each well for 1–4 hrs of incubation and the supernatant was collected in a 96-well plate. The absorbance was measured by a spectrophotometer (Bio Tek Instruments Inc., VT, USA) at 450 nm.

Biological evaluation in vivo

Surgical implantation of animal study

A total of 20 male Sprague Dawley rats (5–6 weeks old, average weight: 150 g) were used in our study, obtained from the Laboratory Animal Center of Tongji Medical College, Huazhong University of Science and Technology. The Ethics Committee of animal experimentation of Huazhong University of Science and Technology approved and reviewed the protocol on rats. Besides, the experimental rats were treated in adherence to the Guide for the Care and Use of Laboratory Animals (8th edition). The surgical procedure was based on our previous studies.[6,23] Briefly, the rats were randomly divided into five subgroups: group Ⅰ (Ti), group Ⅱ (TiO_2 NRDs), group Ⅲ (TiO_2@PDA NRDs), group Ⅳ (Ag-TiO_2 NRDs), and group Ⅴ (Ag-TiO_2@PDA NRDs). Before surgery, the rats were anesthetized with pentobarbital (50 mg per 1,000 g body weight) by intraperitoneal injection. An incision was made along the right knee to expose the proximal metaphysis of the anterior tibia, after shaving and disinfecting. Then, a sterilized 20 g syringe needle was used to drill a hole and create a channel through the cortex from the tibia plateau to the medullary cavity. Subsequently, 30 μL bacteria suspension (MASA, 1.5×10^6 CFUs/mL) was injected into the exposed tibia hole using a micro-syringe. Few minutes later, the rod samples of relative groups were implanted into the cavities and the drilled hole was sealed by the sterilized bone wax to prevent leakage of the bacteria suspension. The skin and muscle fascias were sutured firmly at last. In the early stage of recovery, the health conditions of rats including body weight, temperature, and activity were monitored every 24 hrs.[24]

X-ray and micro-CT evaluation

For the sake of evaluating the long-term infection symptoms of the rats, the X-ray examination (Kodak, DirectView, DR3000) with the human hand imaging parameter was scanned at 2 and 4 weeks post-surgery after anesthetized. High-resolution micro-computed tomography (I-CT 80 scanner Scanco Medical, Bassersdorf, Switzerland) was used to scan and evaluate the microstructure of the right tibiae at 300 ms, 70 kV, and 114 mA at 2 and 4 weeks after surgery.

Histopathological analysis

All rats were euthanized after 4 weeks. The right tibias with implants were removed and fixed in 4% buffered formalin for 24 hrs. Then, specimens were decalcified in 10% EDTA for one month, embedded in paraffin and further cut into 10-mm sections. The H&E staining and Gram's staining methods were chosen for the histopathological analysis and the images were captured on a light microscopy (Nikon E600, Japan).

Statistical analysis

The experiments were repeated in triplicate using independent samples, and the results were represented as mean ± standard deviation. A one-way ANOVA combined with a Turkey's post hoc test was used to assess the considered statistical significance; a value of $p<0.05$ was considered significant.

Results

Morphology, structure, and surface characterization

Figure 2A displays the FE-SEM images of Ti, TiO_2 NRDs, TiO_2@PDA NRDs, Ag-TiO2 NRDs, and Ag-TiO_2@PDA NRDs, respectively. As shown in Figure 2A, the quasi-aligned TiO_2 NRDs with diameters of about 50–100 nm and lengths of 1–2 μm are fabricated by a simple hydrothermal reaction with Ti foils. Followed by the self-polymerization of PDA, the

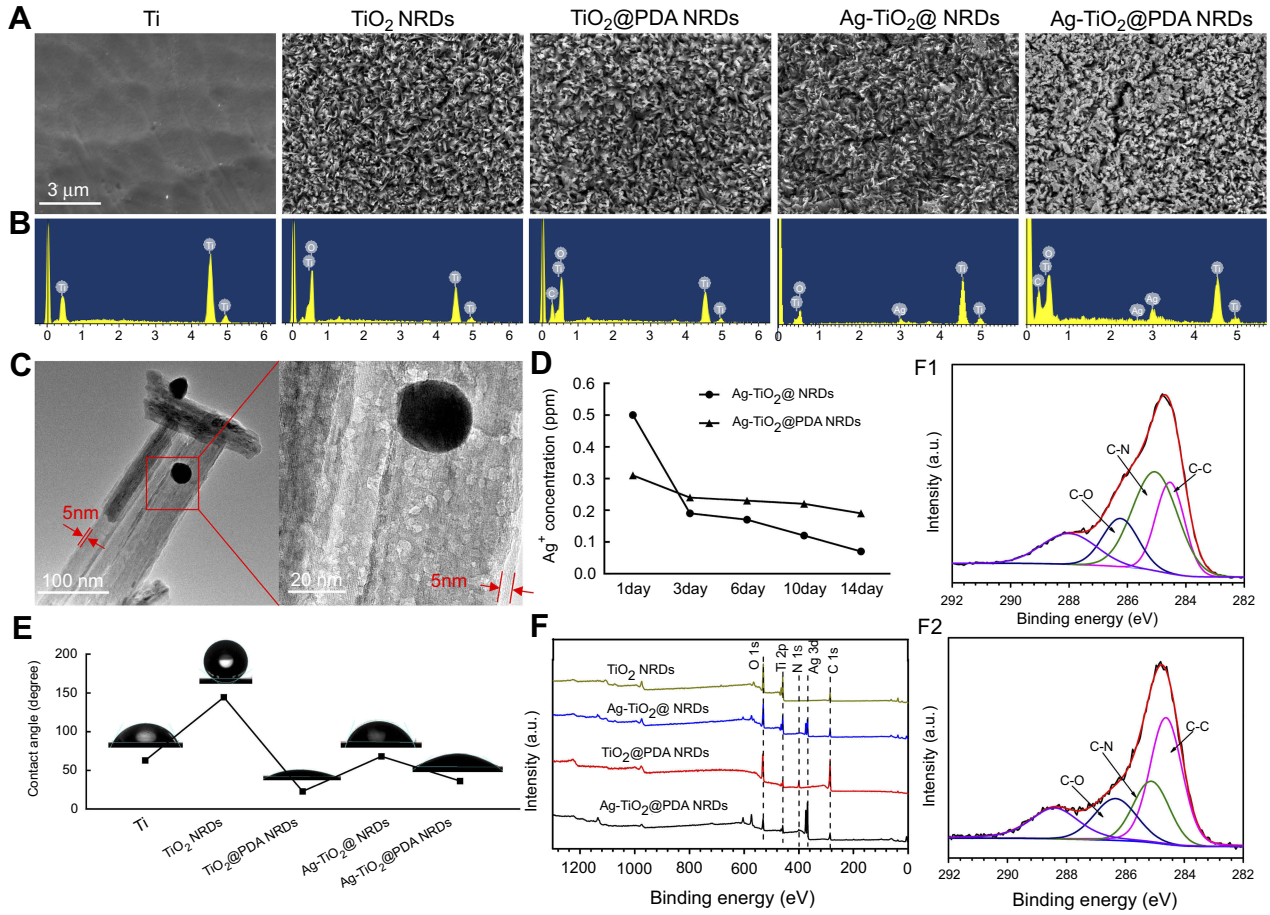

Figure 2 Sample surface characterization and Ag^+ ions release. (**A**) FE-SEM images of various surfaces (scale bars =3 μm); (**B**) corresponding EDS spectrum of various samples; (**C**) TEM images of Ag-TiO_2@PDA NRDs (scale bars =100 [left panel] and 20 [right panel] nm); (**D**) Ag-release profiles from Ag-TiO2 NRDs and Ag-TiO_2@PDA NRDs into PBS; (**E**) water contact angles and photographs of water droplets on various surfaces; (**F**) XPS spectra of various samples; (F1) C 1s peak of Ag-TiO2 NRDs; (F2) C 1s peak of Ag-TiO_2@PDA NRDs.

NRDs surface represented an increased thickness of approximately 5 nm which was shown in the TEM image, while the needle-shaped morphology did not appear deformed (Figure 2C). An average size of embedded Ag nanoparticles nearly 30 nm was confirmed by using TEM (Figure 2C). The corresponding EDX spectrum (Figure 2B) and the XPS spectra (Figure 2F) showed that C, O, Ti, N, and Ag existed in the sample of Ag-TiO_2@PDA NRDs, indirectly demonstrating the formation of TiO_2 NRDs incorporated with PDA and Ag nanoparticles. The XPS spectra of Ag3d peaks were detected at 368.3 and 374.3 eV, respectively, suggesting the presence of Ag on the layer of NRDs. Besides, the release kinetics of Ag-TiO_2 NRDs and Ag-TiO_2@PDA NRDs are shown in Figure 2D that the concentrations of released Ag^+ ions were 0.50, 0.19, 0.17, 0.12, and 0.07 ppm for Ag-TiO_2 NRDs and 0.31, 0.24, 0.23, 0.22, and 0.19 ppm for Ag-TiO_2@PDA NRDs at 1, 3, 6, 10, and 14 days, respectively. Because of refreshing the soaking liquid every 24 hrs, we observed a burst-release pattern of Ag^+ ions in Ag-TiO_2 NRDs group by ICP-AES in the first 3 days. On the contrary, the release pattern of Ag^+ ions in Ag-TiO_2@PDA NRDs group was much slower and more gentle. The contact angles of Ti, TiO_2 NRDs, TiO_2@PDA NRDs, Ag-TiO2 NRDs, and Ag-TiO_2 @PDA NRDs were 62.9°, 144.4°, 22.7°, 68.1°, and 36.4°, respectively (Figure 2E). The nitrogen-to-carbon (N/C) ratio of 12.56% (8.1% for nitrogen; 64.48% for carbon) of TiO_2@PDA NRDs determined by XPS was same to the theoretical N/C for dopamine,[13,25] further indicating that TiO_2 NRDs were modified with PDA. As the high-resolution spectra shown in Fig. 2F1 and F2, the C 1s peaks of TiO_2@PDA NRDs and Ag-TiO_2 @PDA NRDs can be deconvoluted into subpeaks at 284.6, 285.1, and 286.3 eV corresponding to C-C, C-N, and C-O, respectively.[26]

Antibacterial activity in vitro

The antibacterial activities against MRSA and *E. coli* were measured by FE-SEM, Live/Dead staining, ZOI, bacteria counting method, and protein leakage analysis in vitro.

After incubation for 24 hrs, the morphology of the adherent MRSA and *E. coli* was measured by FE-SEM in Figure 3A and B, respectively. MRSA presented spherical on pure Ti, but irregular and lysed on Ag-TiO_2 NRDs and Ag-TiO_2@PDA NRDs surfaces. Similarly, *E. coli* became corrugated, distorted, and lysed on Ag-TiO_2 NRDs and Ag-TiO_2@PDA NRD surfaces.

The live/dead staining assay is shown in Figure 3C and D. The biofilm was formed on the complete coverage of pure Ti group at 48 hrs. However, the amount of bacteria coverage on NRDs samples was considerably lower than that on pure Ti group. Moreover, many yellow and red

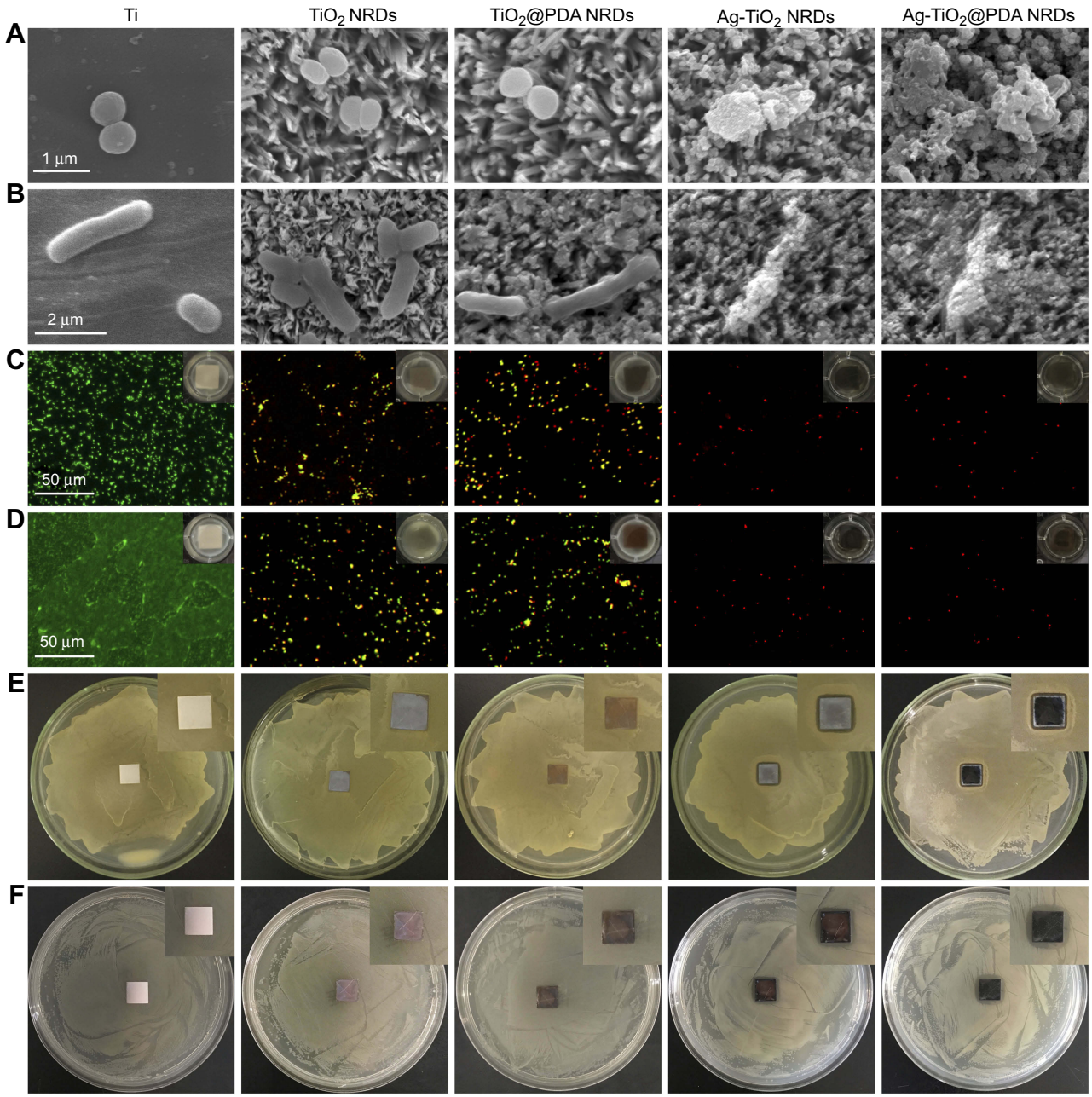

Figure 3 Antibacterial activity in vitro. (**A**) FE-SEM morphology of *methicillin-resistant Staphylococcus aureus* (MRSA) seeded on the various surfaces (scale bars =1 μm); (**B**) FE-SEM morphology of *Escherichia coli* (*E. coli*) seeded on the various surfaces (scale bars =2 μm); (**C**) fluorescent images of stained MRSA and bacterial suspension (insert in part C) after co-cultured with various surfaces for 24 hrs (scale bars =50 μm); (**D**) fluorescent images of stained MRSA and bacterial suspension (insert in part D) after co-cultured with various surfaces for 48 hrs (scale bars =50 μm); (**E**) zone of inhibition (ZOI) test of the various coatings against MRSA; (**F**) ZOI test of the various coatings against *E. coli.*

spots can be observed from TiO_2 NRDs and TiO_2@PDA NRDs group, indicating significantly physical punctured of bacteria membrane. Almost all red spots can be observed from Ag-TiO_2 NRDs and Ag-TiO_2@PDA NRDs, indicating more dead bacteria and admirable antibacterial ability.

As shown in Figure 3E and F, the ZOI diameters of Ag-TiO_2 NRDs for MRSA and *E. coli* were 13.2±0.2 mm and 15.9±1.6 mm, respectively. The ZOI diameters of Ag-TiO_2@PDA NRDs for MRSA and *E. coli* were 13.5 ±0.5 mm and 16.1±1.3 mm, respectively.

The anti-adherent bacterial activity against MRSA and *E. coli* was evaluated by the bacteria counting method. Compared to the pure Ti group, Ag-TiO_2 NRDs and Ag-TiO_2@PDA NRDs showed adequate bactericidal effect. Ag-TiO_2 NRDs showed the antibacterial rates of 97.1 ±1.0%, 59.8±3.9%, and 34.3±12.0% against MRSA (Figure 4A) and 98.2±1.0%, 83.5±2.1%, and 37.2±5.9% against *E. coli* at 1, 7, and 14 days (Figure 4B), respectively. However, Ag-TiO_2@PDA NRDs showed longer-term antibacterial effects, with antibacterial rates of 95.4±2.0%, 88.6 ±1.5%, and 80.1±1.1% against MRSA (Figure 4A) and 96.7 ±2.1%, 91.3±0.5%, and 86.2±2.6% against *E. coli* at 1, 7, and 14 days (Figure 4B), respectively. Interestingly, TiO_2 NRDs (22.3±3.9% for MRSA and 25.4±12.3% for *E. coli*) and TiO_2@PDA NRDs (24.5±2.4% for MRSA and 23.1 ±7.2% for *E. coli*) group also have the anti-adherent bacterial ability compared with the pure Ti group (Figure 4C).

As shown in Figure 5A, the protein leakage concentration of Ti, TiO_2 NRDs, TiO_2@PDA NRDs, Ag-TiO2 NRDs, and Ag-TiO_2@PDA NRDs was 262.5±5.5, 307.5 ±17.8, 305.7±9.5, 398.2±2.8, and 364.9±2.8 μg/mL for MRSA and 263.8±2.8, 296.4±5.9, 285.3±8.7, 364.3±6.4, and 359.9±10.2 μg/mL for *E. coli*, respectively.

Cell adhesion, morphology, and cytotoxicity in vitro

As shown in Figure 6A and B, the pure Ti had a low affinity to osteoblasts with the spherical morphology. In contrast, the polygonal shape and distinct pseudopodia of MC3T3-E1 were observed on TiO_2 NRDs and TiO_2@PDA NRDs reflecting the adequate cellular adhesion and extension. However, the different degrees of cell shrinkage were observed on the Ag-TiO_2 NRDs surfaces, probably because of the burst release of Ag^+ ions. With the PDA coatings, the extensive morphology of cells was detected on Ag-TiO_2@PDA NRDs samples, confirming that the cytotoxicity of Ag^+ ions can be sharply reduced through the combination by PDA.

Similar to FE-SEM morphology, the cell morphology, adhesion, and spreading activity were measured by immunofluorescence to visualize the cytoskeleton and nuclei, respectively (Figure 6C). Compared to the pure Ti and Ag-TiO_2 NRDs group, TiO_2 NRDs, TiO_2@PDA NRDs, and Ag-TiO_2@PDA NRDs promoted cell extension and cell spreading. The shrinking cells on the Ag-TiO_2 NRD surfaces implied the inevitable cytotoxicity of Ag^+ ions.

Furthermore, we used a CCK-8 assay kit to investigate the cytotoxicity level for cell cultures on various samples

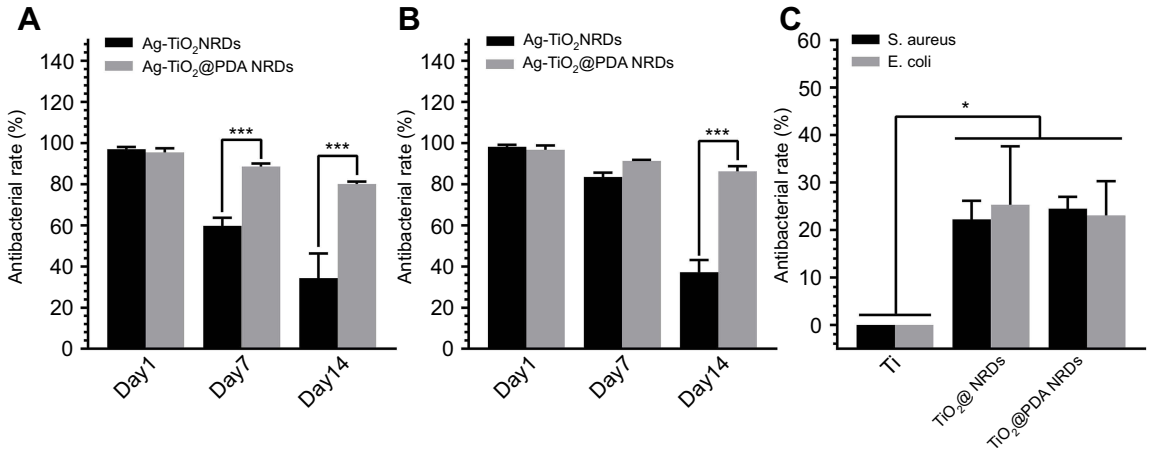

Figure 4 Anti-adherent bacterial activity in vitro. (**A**) *Methicillin-resistant Staphylococcus aureus* (MRSA) recultured on agar after dissociation from Ag-TiO2 NRDs and Ag-TiO_2@PDA NRDs at day 1, day 7, and day 14; (**B**) *Escherichia coli* (*E. coli*) recultured on agar after dissociation from Ag-TiO2 NRDs and Ag-TiO_2@PDA NRDs at day 1, day 7, and day 14; (**C**) MRSA and *E. coli* recultured on agar after dissociation from Ti, TiO_2 NRDs, and TiO_2@PDA NRDs at day 1. The error bars indicate means ± standard deviations: *p<0.05 and ***p<0.001.

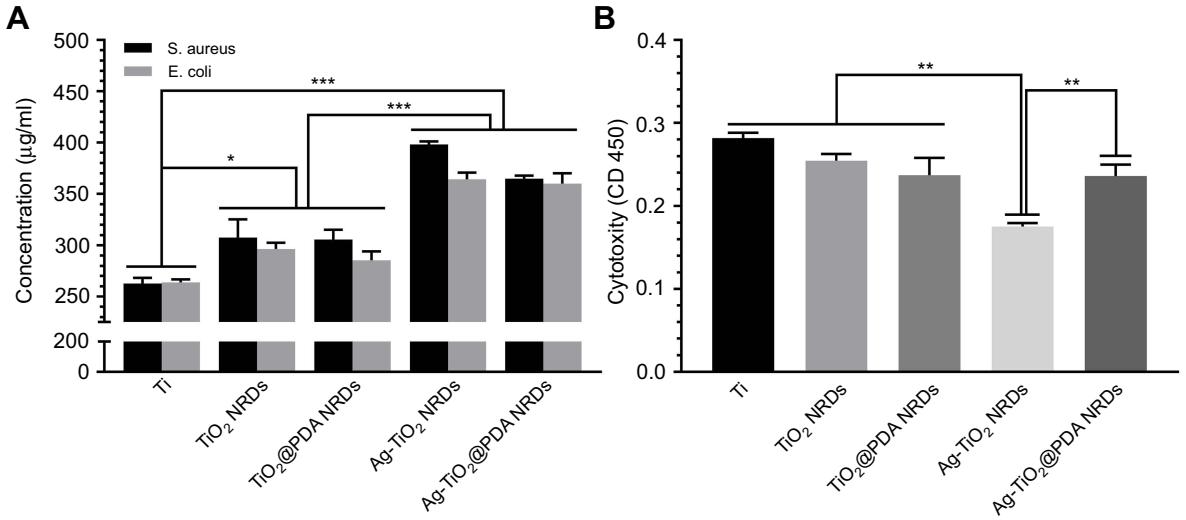

Figure 5 Protein leakage analysis and cytotoxicity evaluation in vitro. (**A**) Concentration of leaked protein in the supernatant of various groups; (**B**) cytotoxicity level of various surfaces by CCK-8 test. The error bars indicate means ± standared deviations: *p<0.05, ** p<0.01, and ***p<0.001.

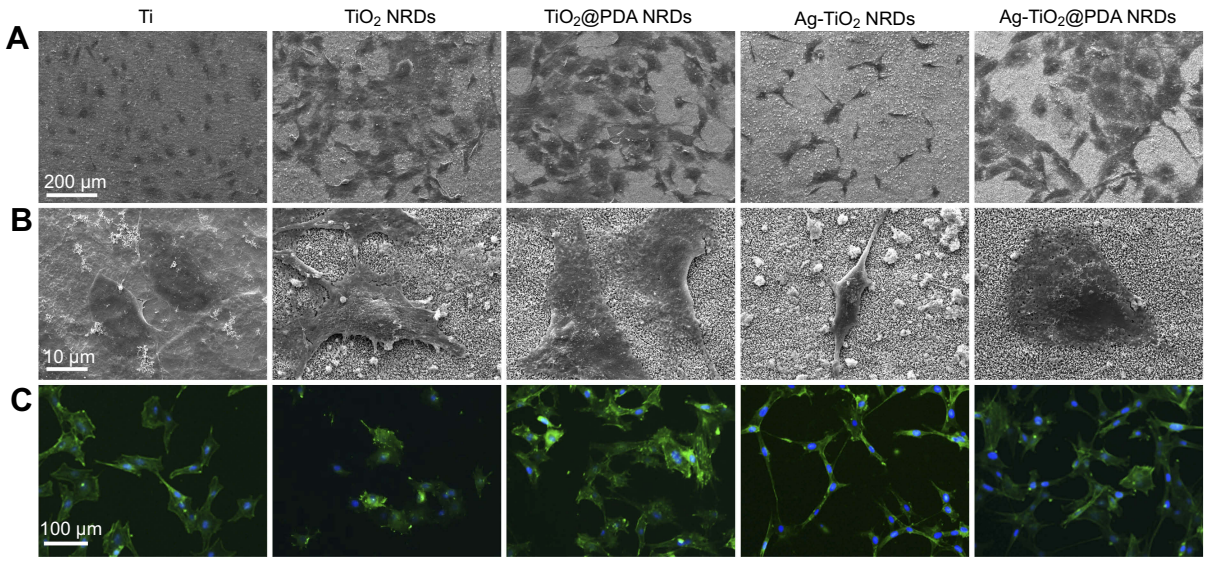

Figure 6 Cell morphology in vitro. (**A, B**) FE-SEM cell morphology of mouse calvarial cells (MC3T3-E1) cells cultured on various surfaces for 24 hrs (scale bars =200 [**A**] and 10 [**B**] μm); (**C**) fluorescent images of MC3T3-E1 cells cultured on various surfaces for 24 hrs with phalloidion (green) and DAPI (blue) (scale bars =100 μm).

(Figure 5B). Compared with Ti, TiO_2 NRDs, TiO_2@PDA NRDs, and Ag-TiO_2@PDA NRDs, the Ag-TiO_2 NRDs samples exhibited the highest cytotoxicity (** p<0.01). Besides, the absorbance of Ag-TiO_2@PDA NRDs group showed no significant difference with the absorbance of TiO_2 NRDs and TiO_2@PDA NRDs groups (p>0.05).

In vivo antibacterial assay

As shown in Figure 7A, X-ray images were taken at 2 and 4 weeks after surgery. Two weeks after surgery, a classic symptom of implant infection like osteolysis (red arrows), architectural deformation, periosteal reactions (white arrows), and soft tissue deformation was visible in group Ⅰ, group Ⅱ, and group Ⅲ. Four weeks after surgery, extensive osteolysis (red arrows) and fibrosis of bone marrow cavity was observed in group Ⅰ, group Ⅱ, and group Ⅲ. In contrast, no signs of infection were observed in groups Ⅳ and Ⅴ.

Micro CT scanning was used to analyze the samples (Figure 7B). Two weeks after surgery, the obvious sequestrum (white arrows) was detected in group Ⅰ, group Ⅱ, and group Ⅲ. Four weeks after surgery, the involucrum was formed and the sequestrum (white arrows) was partially resolved in group Ⅰ, group Ⅱ, and group Ⅲ. Similar

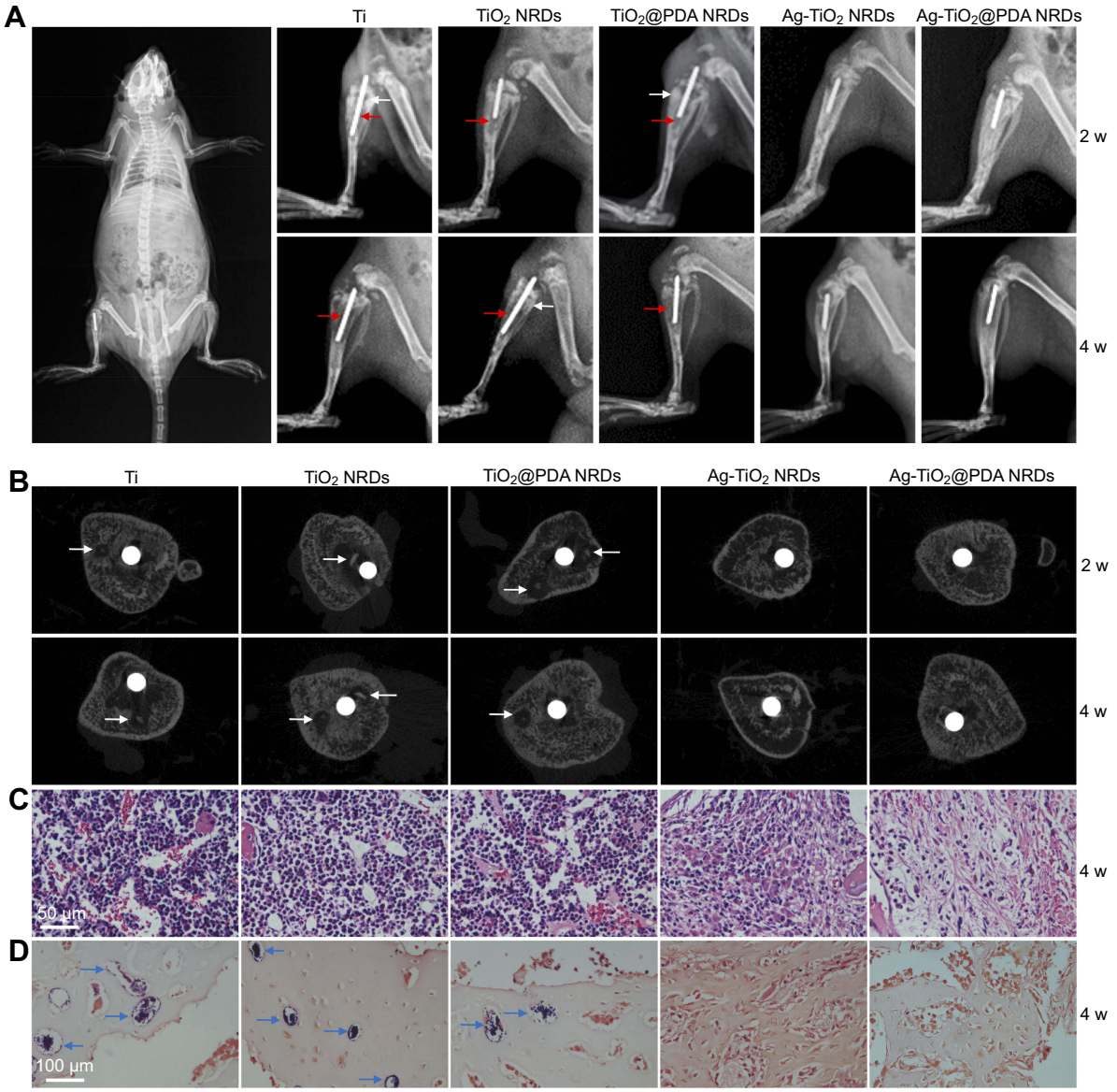

Figure 7 Implant infection model in vivo. (**A**) X-ray examination of the osteomyelitis model implanted with Ti rod 1 hr after surgery (left panel) and different kinds of rods at 2 weeks and 4 weeks (right panel), red arrows indicate osteolysis, white arrows indicate periosteal reaction; (**B**) cross-sectional images of micro-CT of different samples at 2 weeks and 4 weeks, white arrows indicate sequestrum; (**C**) H&E stain of different samples at 4 weeks (scale bars =50 μm); (**D**) gram stain of different samples at 4 weeks (scale bars =100 μm), blue arrows indicate MRSA colonies.

to the X-ray results, no sign of infection was detected in groups Ⅳ and Ⅴ.

In Figure 7C, histological analysis showed that abundant and excessive neutrophil infiltration accompanied with abscess and necrotic cells was observed at 4 weeks in groups Ⅰ, Ⅱ, and Ⅲ. Gram staining in Figure 7D showed that the stained bacteria (blue arrows) were gathering around sequestrum or micro-abscesses. However, negligible inflammatory infiltration and absence of bacteria were observed in group Ⅳ or Ⅴ at 4 weeks.

Discussion

The bacterial infection, mainly caused by gram-positive *S. aureus* and gram-negative *E. coli*, usually becomes a devastating blow for the orthopedic and dental surgery, leading to inevitable implant failure and secondary surgery.[4,6,7] In our study, we successfully utilized the method of hydrothermal synthesis to produce Ag-TiO_2@PDA NRDs coatings on Ti substrates, which possessed an adequate long-term antibacterial ability and anti-biofilm activities with satisfied biocompatibility in vitro and in vivo. Therefore, this novel surface strategy may be

expected for the biomedical applications in the future clinical implants.

The potential synergistic anti-bacterial mechanisms of Ag-TiO_2@PDA NRDs might have three aspects. Firstly, the needle-like NRDs can selective physical puncture the bacteria cell wall because of fewer anchoring sites, less contact area, and higher contact pressure between the NRDs and the bacteria, leading to the severely damaged of membrane (FE-SEM and Live/Dead Bacterial Viability fluorescence) and the significant cytoplasm leakage (the quantitative protein analysis test) of bacteria cells.[21,22,26] In our Live/Dead Bacterial Viability fluorescence test, the intact and damaged bacterial membranes could be stained by SYTO 9 (green), while propidium iodide (red) only penetrated and stained cells with damaged membranes, causing a reduction of SYTO 9 stain. Thus, NRDs have been proved to have the ability of selectively physically puncturing the bacterial membrane according to more yellow and red spots observed from TiO_2 NRDs and TiO_2 @PDA NRDs group. In addition, the quantitative protein analysis test showed that the protein leakage concentration of TiO_2 NRDs, TiO_2@PDA NRDs, Ag-TiO2 NRDs, and Ag-TiO_2@PDA NRDs groups was significantly higher than that of Ti group, which added another evidence of physical bacteria membrane puncture. However, MC3T3-E1 exhibited good adherence and spreading behavior with the polygonal shape and distinct pseudopodia on NRDs surfaces. This is probably due to an approximate order of magnitude difference in the size of morphology.[26]

Secondly, Ag^+ ions released from the Ag nanoparticles have the excellent bactericidal effect (ZOI and the bacteria counting method). The results of ZOI showed that Ag-TiO 2 NRDs and Ag-TiO_2@PDA NRDs both exhibited high-efficient antibacterial activity (13.2±0.2 mm for MRSA and 15.9±1.6 mm for *E. coli* in Ag-TiO_2 NRDs; 13.5 ±0.5 mm for MRSA and 16.1±1.3 mm for *E. coli* in Ag-TiO_2@PDA NRDs). The contributing bactericidal mechanisms may include the inhibition and disruption of bacterial cell wall synthesis, reactive oxygen species forming, protein denaturation, and DNA damaging.[27,28] Aside from its bactericidal actions, Ag can also completely restrict the growth of resistant strains.[29,30]

Thirdly, the topography of submicron and microsized surface can prevent the biofilm formation (FE-SEM, Live/Dead Bacterial Viability fluorescence, and the bacteria counting method).[31–33] In comparison to the patterned surface, it was reported that bacteria were more likely to attach on smoother ones.[31,34–36] Thus, the results of Live/Dead Bacterial Viability fluorescence showed that the amount of bacteria coverage on NRDs samples was significantly lower than that on the pure Ti group on which the typical biofilm was formed after 48 hrs.

In our study, the self-polymerization of PDA was coated on the NRDs to modulate the Ag^+ ions release kinetics, improve the hydrophilicity of the surface, and promote the biocompatibility of Ag-TiO_2@PDA NRDs. A large concentration of Ag^+ ions can generate a considerable level of cytotoxicity and affect tissue formation. Unlike the burst-release pattern of Ag^+ ions observed by ICP-AES in Ag-TiO_2 NRDs group in the first 3 days, the PDA of Ag-TiO_2@PDA NRDs coatings can bind to Ag^+ ions more stably via the effect of chelation and modify the release kinetics of Ag^+ ions to reduce the cytotoxicity and improve the biocompatibility. In addition, the antibacterial property of Ag-TiO_2@PDA NRDs was significantly more durable and efficient than that of Ag-TiO_2 NRDs, according to the results of the bacteria counting method (88.6±1.5% vs 59.8±3.9% on day 7 and 80.1 ±1.1% vs 34.3±12.0% on day 14 against MRSA; 86.2 ±2.6% vs 37.2±5.9% on day 14 against *E. coli*). It is implied that the controlled Ag^+ ions release by the chelation effect of PDA almost completely preserved the long-term bactericidal ability. Meanwhile, owing to the particular surface nanostructure and lower surface free energy, the NRDs surface with the water contact angle of 144.4° exhibited the considerable hydrophobic property.[37] After coating with PDA, Ag-TiO_2@PDA NRDs showed the hydrophilicity of 36.4°, which improved the wettability of NRDs and was more conducive to cell adhesion, proliferation, osteoblast differentiation, and osteogenesis.[38,39] In addition, the micro- or nano-textured topography and roughness of implant surface have been also reported to affect the cell morphology, proliferation, and differentiation of stem cell.[40,41] Well-spread pre-osteoblasts with a mature cell shape and larger surface area are more accessible to ossification differentiation.[42,43] Thus, the special ability of the NRDs coatings to promote cell adherence and spreading may eventually enhance the bone regeneration. In general, considering the balance of cytotoxicity and long-term antibacterial effects, we demonstrate that the abilities of PDA coatings will highlight the promising potential for the application in Ag-based tissue engineering.

Modern medical imaging technologies, such as X-ray and CT, have been widely used in the diagnosis of bone infection.[44] In order to further test the bactericidal ability of

Ag-TiO_2@PDA NRDs in vivo, we successfully conducted a rat model of osteomyelitis following a previously established protocol, which subsequently observed the radiographic signs of osteomyelitis by X-ray and micro-CT at 2 and 4 weeks and analyzed the histopathology by H&E and Gram's staining at 4 weeks. The consistent results of imaging and histopathology demonstrated that the injected MRSA was killed by the Ag^+ ions–loaded coatings. Consequently, the Ag-TiO_2@PDA NRDs coatings possessed a convincing antibacterial ability, which was highly recommended for the developing clinical applications.

One limitation needs to be mentioned. The different sizes, shapes, and concentrations of Ag nanoparticles may lead to the change of dissolution kinetics.[45] For example, a decrease in the size of Ag nanoparticles may increase the speed of Ag^+ ions dissolution.[46] Thus, finding the proper size, shape, and concentration of Ag nanoparticles requires further research.

Conclusion

We successfully fabricated the Ag-TiO_2@PDA NRDs coatings on Ti substrates by the method of hydrothermal synthesis. The Ag-TiO_2@PDA NRDs coatings with the synergistic effect of selective physical punctual and controlled Ag^+ ions release achieved an adequate long-term antibacterial and anti-biofilm activities against MRSA and *E. coli* with satisfied biocompatibility in vitro and in vivo. Meanwhile, with relatively simple, economical, and suitable fabrication method, the Ag-TiO_2@PDA NRDs coatings may be hopeful for the applications of orthopedic and dental implants.

Acknowledgments

This work is supported by National Natural Science Foundation of China (No. 81571816 and 81601611). Ming Guan is also supported by a fellowship from the China Scholarship Council.

Disclosure

There are no potential conflicts of interest for the authors to disclose in this work.

References

1. Sidambe AT. Biocompatibility of advanced manufactured titanium implants: a review. *Materials (Basel, Switzerland)*. 2014;7(12):8168–8188. doi:10.3390/ma7128168
2. Raphel J, Holodniy M, Goodman SB, Heilshorn SC. Multifunctional coatings to simultaneously promote osseointegration and prevent infection of orthopaedic implants. *Biomaterials*. 2016;84:301–314. doi:10.1016/j.biomaterials.2016.01.016
3. Tobin EJ. Recent coating developments for combination devices in orthopedic and dental applications: a literature review. *Adv Drug Delivery Rev*. 2017;112:88–100. doi:10.1016/j.addr.2017.01.007
4. Vielgut I, Sadoghi P, Wolf M, et al. Two-stage revision of prosthetic hip joint infections using antibiotic-loaded cement spacers: when is the best time to perform the second stage? *Int Orthop*. 2015;39(9):1731–1736. doi:10.1007/s00264-015-2751-5
5. Cheng H, Xiong W, Fang Z, et al. Strontium (Sr) and silver (Ag) loaded nanotubular structures with combined osteoinductive and antimicrobial activities. *Acta Biomater*. 2016;31:388–400. doi:10.1016/j.actbio.2015.11.046
6. Xu N, Cheng H, Xu J, et al. Silver-loaded nanotubular structures enhanced bactericidal efficiency of antibiotics with synergistic effect in vitro and in vivo. *Int J Nanomed*. 2017;12:731–743. doi:10.2147/IJN.S123648
7. Darley ES, MacGowan AP. Antibiotic treatment of gram-positive bone and joint infections. *J Antimicrob Chemother*. 2004;53(6):928–935. doi:10.1093/jac/dkh191
8. Anselme K, Davidson P, Popa AM, Giazzon M, Liley M, Ploux L. The interaction of cells and bacteria with surfaces structured at the nanometre scale. *Acta Biomater*. 2010;6(10):3824–3846. doi:10.1016/j.actbio.2010.04.001
9. Cloutier M, Mantovani D, Rosei F. Antibacterial coatings: challenges, perspectives, and opportunities. *Trends Biotechnol*. 2015;33(11):637–652. doi:10.1016/j.tibtech.2015.09.002
10. Amin Yavari S, van der Stok J, Chai YC, et al. Bone regeneration performance of surface-treated porous titanium. *Biomaterials*. 2014;35(24):6172–6181. doi:10.1016/j.biomaterials.2014.04.054
11. Lee YH, Cheng FY, Chiu HW, et al. Cytotoxicity, oxidative stress, apoptosis and the autophagic effects of silver nanoparticles in mouse embryonic fibroblasts. *Biomaterials*. 2014;35(16):4706–4715. doi:10.1016/j.biomaterials.2014.02.021
12. Kumar R, Munstedt H. Silver ion release from antimicrobial polyamide/silver composites. *Biomaterials*. 2005;26(14):2081–2088. doi:10.1016/j.biomaterials.2004.05.030
13. Lee H, Dellatore SM, Miller WM, Messersmith PB. Mussel-inspired surface chemistry for multifunctional coatings. *Science*. 2007;318(5849):426–430. doi:10.1126/science.1147241
14. Liu Y, Ai K, Lu L. Polydopamine and its derivative materials: synthesis and promising applications in energy, environmental, and biomedical fields. *Chem Rev*. 2014;114(9):5057–5115. doi:10.1021/cr400407a
15. Ho Cc, Ding Sj. Structure, properties and applications of mussel-inspired polydopamine. *J Biomed Nanotechnol*. 2014;10(10):3063–3084.
16. Lynge ME, van der Westen R, Postma A, Stadler B. Polydopamine – a nature-inspired polymer coating for biomedical science. *Nanoscale*. 2011;3(12):4916–4928. doi:10.1039/c1nr10969c
17. Ye Q, Zhou F, Liu W. Bioinspired catecholic chemistry for surface modification. *Chem Soc Rev*. 2011;40(7):4244–4258. doi:10.1039/c1cs15026j
18. Ku SH, Park CB. Human endothelial cell growth on mussel-inspired nanofiber scaffold for vascular tissue engineering. *Biomaterials*. 2010;31(36):9431–9437. doi:10.1016/j.biomaterials.2010.08.071
19. Ku SH, Lee JS, Park CB. Spatial control of cell adhesion and patterning through mussel-inspired surface modification by polydopamine. *Langmuir*. 2010;26(19):15104–15108. doi:10.1021/la102825p
20. Meng J, Zhang P, Wang S. Recent progress in biointerfaces with controlled bacterial adhesion by using chemical and physical methods. *Chem Asian J*. 2014;9(8):2004–2016. doi:10.1002/asia.201402200
21. Ivanova EP, Hasan J, Webb HK, et al. Natural bactericidal surfaces: mechanical rupture of *Pseudomonas aeruginosa* cells by cicada wings. *Small (Weinheim an Der Bergstrasse, Germany)*. 2012;8(16):2489–2494. doi:10.1002/smll.201200528

22. Ivanova EP, Hasan J, Webb HK, et al. Bactericidal activity of black silicon. *Nat Commun*. 2013;4:2838. doi:10.1038/ncomms3838
23. Cheng H, Li Y, Huo K, Gao B, Xiong W. Long-lasting in vivo and in vitro antibacterial ability of nanostructured titania coating incorporated with silver nanoparticles. *J Biomed Mater Res Part A*. 2014;102 (10):3488–3499. doi:10.1002/jbm.a.35019
24. Nicklas W, Baneux P, Boot R, et al. Recommendations for the health monitoring of rodent and rabbit colonies in breeding and experimental units. *Labor Animals*. 2002;36(1):20–42. doi:10.1258/0023677021911740
25. Lee H, Rho J, Messersmith PB. Facile conjugation of biomolecules onto surfaces via mussel adhesive protein inspired coatings. *Adv Mater*. 2009;21(4):431–434. doi:10.1002/adma.200801222
26. Li J, Tan L, Liu X, et al. Balancing bacteria-osteoblast competition through selective physical puncture and biofunctionalization of ZnO/polydopamine/arginine-glycine-aspartic acid-cysteine nanorods. *ACS Nano*. 2017;11(11):11250–11263. doi:10.1021/acsnano.7b05620
27. Franci G, Falanga A, Galdiero S, et al. Silver nanoparticles as potential antibacterial agents. *Molecules*. 2015;20(5):8856–8874. doi:10.3390/molecules20058856
28. Duran N, Duran M, de Jesus MB, Seabra AB, Favaro WJ, Nakazato G. Silver nanoparticles: a new view on mechanistic aspects on antimicrobial activity. *Nanomed Nanotechnol Biol Med*. 2016;12 (3):789–799. doi:10.1016/j.nano.2015.11.016
29. Ahmed S, Ahmad M, Swami BL, Ikram S. A review on plants extract mediated synthesis of silver nanoparticles for antimicrobial applications: a green expertise. *J Adv Res*. 2016;7(1):17–28. doi:10.1016/j.jare.2015.02.007
30. Panacek A, Smekalova M, Kilianova M, et al. Strong and nonspecific synergistic antibacterial efficiency of antibiotics combined with silver nanoparticles at very low concentrations showing no cytotoxic effect. *Molecules*. 2015;21(1):E26. doi:10.3390/molecules21010026
31. Zhang B, Luo Y, Pearlstein AJ, et al. Fabrication of biomimetically patterned surfaces and their application to probing plant-bacteria interactions. *ACS Appl Mater Interf*. 2014;6(15):12467–12478. doi:10.1021/am502384q
32. Burgers R, Gerlach T, Hahnel S, Schwarz F, Handel G, Gosau M. In vivo and in vitro biofilm formation on two different titanium implant surfaces. *Clin Oral Implants Res*. 2010;21(2):156–164. doi:10.1111/j.1600-0501.2009.01815.x
33. Crawford RJ, Webb HK, Truong VK, Hasan J, Ivanova EP. Surface topographical factors influencing bacterial attachment. *Adv Colloid Interf Sci*. 2012;179-182:142–149. doi:10.1016/j.cis.2012.06.015
34. Ge X, Leng Y, Lu X, et al. Bacterial responses to periodic micropillar array. *J Biomed Mater Res Part A*. 2015;103(1):384–396. doi:10.1002/jbm.a.35182
35. Valle J, Burgui S, Langheinrich D, et al. Evaluation of surface microtopography engineered by direct laser interference for bacterial anti-biofouling. *Macromol Biosci*. 2015;15(8):1060–1069. doi:10.1002/mabi.201500107
36. Vasudevan R, Kennedy AJ, Merritt M, Crocker FH, Baney RH. Microscale patterned surfaces reduce bacterial fouling-microscopic and theoretical analysis. *Colloids Surf B Biointerf*. 2014;117:225–232. doi:10.1016/j.colsurfb.2014.02.037
37. Xiang Y, Li J, Liu X, Cui, Z., Yang, X., Yeung, K.W.K., Pan, H., Wu, S. Construction of poly(lactic-co-glycolic acid)/ZnO nanorods/Ag nanoparticles hybrid coating on Ti implants for enhanced antibacterial activity and biocompatibility. *Mater Sci Eng C*. 2017;79:629–637. doi:10.1016/j.msec.2017.05.115
38. Wu S, Liu X, Hu T, et al. A biomimetic hierarchical scaffold: natural growth of nanotitanates on three-dimensional microporous Ti-based metals. *Nano Lett*. 2008;8(11):3803–3808. doi:10.1021/nl802145n
39. Liao H, Andersson AS, Sutherland D, Petronis S, Kasemo B, Thomsen P. Response of rat osteoblast-like cells to microstructured model surfaces in vitro. *Biomaterials*. 2003;24(4):649–654.
40. Xu JY, Chen XS, Zhang CY, Liu Y, Wang J, Deng FL. Improved bioactivity of selective laser melting titanium: surface modification with micro-/nano-textured hierarchical topography and bone regeneration performance evaluation. *Mater Sci Eng C Mater Biol Appl*. 2016;68:229–240. doi:10.1016/j.msec.2016.05.096
41. Huang Q, Elkhooly TA, Liu X, et al. Effects of hierarchical micro/nano-topographies on the morphology, proliferation and differentiation of osteoblast-like cells. *Colloids Surf B Biointerf*. 2016;145:37–45. doi:10.1016/j.colsurfb.2016.04.031
42. Kilian KA, Bugarija B, Lahn BT, Mrksich M. Geometric cues for directing the differentiation of mesenchymal stem cells. *Proc Natl Acad Sci USA*. 2010;107(11):4872–4877. doi:10.1073/pnas.0903269107
43. McBeath R, Pirone DM, Nelson CM, Bhadriraju K, Chen CS. Cell shape, cytoskeletal tension, and RhoA regulate stem cell lineage commitment. *Develop Cell*. 2004;6(4):483–495.
44. Peltola H, Paakkonen M. Acute osteomyelitis in children. *New Engl J Med*. 2014;370(4):352–360. doi:10.1056/NEJMra1213956
45. Chernousova S, Epple M. Silver as antibacterial agent: ion, nanoparticle, and metal. *Angewandte Chemie*. 2013;52(6):1636–1653. doi:10.1002/anie.201205923
46. Liu J, Sonshine DA, Shervani S, Hurt RH. Controlled release of biologically active silver from nanosilver surfaces. *ACS Nano*. 2010;4(11):6903–6913. doi:10.1021/nn102272n